

The role of group velocity delay in Faraday rotation in a multilayer polymer lattice

Michael Crescimanno,¹ Guilin Mao,¹ James H. Andrews,¹ Kenneth D. Singer,^{2,3} Eric Baer,²
Anne Hiltner,^{2#} Hyunmin Song,² Kyle Comeau,¹ Bijayandra Shakya,¹ Aaron Bishop,¹ and
Ryan Livingston¹

¹*Department of Physics & Astronomy, One University Plaza, Youngstown State University,
Youngstown, Ohio 44555 USA*

²*Department of Macromolecular Science and Engineering, 2100 Adelbert Rd, Case Western
Reserve University, Cleveland, Ohio 44106, USA*

³*Department of Physics, Case Western Reserve University, 13900 Euclid Ave, Cleveland, Ohio
44106, USA*

[#]Deceased

**Corresponding author: jandrews@ysu.edu*

We measure and model the spectral dependence of Faraday rotation in one-dimensional lattice structures comprised of co-extruded alternating polymer layers of polymethylmethacrylate and polystyrene. We develop theory that shows that the net Faraday rotation in a symmetric multilayer system is determined not by the total thickness of the constituent materials, but by the time spent in each constituent material as measured by the overall group velocity delay of the structure and the relative energy distribution per material. We compare measured and computed Faraday rotation spectra for these films to theoretical predictions, taking into account ellipticity

as well as layer thickness variations and finite spectral width detection. To measure rotations of these thin, non-magnetic, weak Faraday rotators, we constructed and optimized an apparatus capable of measuring broadband Faraday rotation spectra at 0.001 degree resolution for rotation angles as small as 0.002 degrees.

OCIS codes: *160.3820, 160.4890, 160.5293, 160.5470, 230.2240.*

1. INTRODUCTION

The Faraday effect is the rotation of the polarization of light in the presence of a longitudinal magnetic field. In the conventional description of this rotation in a non-birefringent bulk material, the rotation angle θ_F is a linear function of the transport length through the medium (here, length L in the \hat{z} -direction),

$$\theta_F(\lambda) = \int_0^L V(\lambda, z) B(z) dz = V(\lambda) BL, \quad (1)$$

with the right-most expression applying to homogeneous bulk materials in a uniform longitudinal (i.e., along \hat{z}) magnetic field B . Here, $V(\lambda)$ is the Verdet constant, a property of the bulk material. Due to the non-reciprocal nature of Faraday rotation, when there are multilayer reflections, Eq. (1) clearly does not apply. Most importantly, Eq. (1) fails to account for coherent forward and backward scattering, such as occurs, for example, in the vicinity of the reflection band of a photonic crystal. Standard treatments for a one-dimensional photonic crystal (1D-PC) accomplish this through a 4x4 matrix formalism that coherently combines propagation and polarization rotation effects of each layer in the stack.[1] In this paper we detail measurements of Faraday rotation in a multilayer co-extruded polymer and describe an alternative theoretical approach to understanding the rotation in terms of bulk properties, transport time and mode structure.

In Section 2 we describe the materials and the experimental methods we used to measure the spectral dependence of Faraday rotation in a 1D-PC system fabricated through a co-extrusion process. In order to understand our measured Faraday rotation spectra in Section 3, we describe a quantitative time-based theory for Faraday rotation in that Section and the Appendix that relies on the 2×2 transfer matrix formalism only (i.e., the transport of a single polarization in the absence of the Faraday effect) to determine the group velocity delay and the steady state energy density in the multilayer. The group velocity delay and steady state energy density are then combined (as derived in the Appendix) to give the Faraday rotation from a 1D-PC as simply the sum of the products of the time spent in each species by the Verdet coefficient (written in time units) for that species. This approach provides a novel conceptual basis for understanding the suppression of the Verdet effect within the reflection band. As concluded in Section 4, our 2×2 matrix approach gives a simple and quantitative physical picture for the connection between dispersion, standing wave power and Faraday rotation, which may be useful as researchers formulate targeted approaches for optimizing the structure-property relationships of nonreciprocal processes in photonic crystals.

2. EXPERIMENT

A. Materials and Processes

Interest in multilayer polymer stacks as 1D-PCs has grown in the past decade due to the low-cost, ease-of-processing, and tailorability of these systems.[2] Recent efforts using self-assembly[3] and forced assembly[4] co-extrusion now enable large-scale production of custom one-dimensional structures with hundreds of layers and one or more reflection bands tailored for use in the visible/NIR spectrum.[5] These hold promise for being simpler and faster than

traditionally-used multi-step processing, such as embossing,[6] (nano)imprinting,[7] conventional or soft lithography,[8] or repetitive spin-coating and stacking.[9]

Polymer 1D-PCs have been proposed for device applications that take advantage of the increased interaction time of light at the band edges and band defects to enhance or suppress gain, loss, and nonlinear active processes.[10] For example, polymer 1D-PCs doped with gain media have been investigated as distributed feedback lasers,[11] and the use of nonlinear optical constituents in the multilayer has been proposed to activate changes to the reflection band that enable optical switching and optical limiting.[12] Indeed, any process that depends on the time/path length of interaction of light without regard to the direction of propagation of that light is a candidate for enhancement in a 1D-PC due to multilayer reflections at band edges and at defects within the reflection stop band. As suggested by Eq. (1), Faraday rotation is another such path-length dependent process, and we report on its use as a probe for studying the transport time in a 1D-PC.[13]

Unfortunately, while the co-extrusion process that we use has been shown to be compatible with many different polymer constituents, most polymers show only a very small bulk Faraday effect.[14,15,16] Still, the simplicity of preparation and handling of our system, the high transparency of the materials outside the reflection band, and the new ease of constructing 1D-PCs with large numbers of layers, afford us a useful medium for experimentally and theoretically separating the intrinsic and lattice structural effects contributing to Faraday rotation in a 1D-PC.

There has been significant technological progress in the use of magnetic multilayer materials as optical rotators,[17] including theoretical studies of structures incorporating one or more anomalous ‘defect’ layers within an otherwise quarter-wavelength stack.[18,19,20,21]

These one-dimensional magneto-optic crystals (1D-MO-PCs) have typically been modeled and/or measured using various multilayer configurations consisting of one or two distinct dielectric species (A,B) and/or one or two magnetic species (M), typically iron garnet and other magnetically enhanced materials layered with inorganic dielectric glasses. Layered systems studied include magnetic materials sandwiched within a distributed dielectric Bragg structure $(AB)^aM(BA)^b$, [22,23] or magnetic materials alternated with dielectrics as in $(MA)^a$ or $(MA)^aM^b(MA)^b$, [24,25,26], $(MA)^a(AM)^b(MA)^a$, [27,28] $(M_1M_2)^a$ or even purely magnetic bilayers as in $M_1M_2)^aM_1^b(M_2M_1)^a$. [29,30] (Here, for simplicity, superscripts a and b represent number of layers and, in some cases, half-layers, where the layers in parentheses may be in either order.) The quantitative nature of the connection between rotation and transport indicated below in the non-magnetic case provides insights into the Faraday effect of these magnetic 1D-PC systems as well.

The multilayer systems that we studied consist of alternating layers of poly(methyl-methacrylate) (PMMA) and polystyrene (PS) fabricated by a layer-multiplying co-extrusion process previously described in Refs. [4], [11] and [31]. Briefly, the multilayer fabrication process involves feeding the polymer melts into a co-extrusion feed block and then into a series of n multiplying elements, thereby producing large area films with 2^{n+1} layers that can be folded or stacked to create simple defect structures. In our experiments, we measured the transmission and Faraday rotation for a 128-layer $(PS/PMMA)^{64}$ film. The difference of the refractive indices n of PS ($n_D = 1.592 \pm 0.002$) and PMMA ($n_D = 1.491 \pm 0.002$) and average layer thickness of ~ 83 nm caused the multilayer films to display a reflection band around 500-510 nm. We also measured a $(PS/PMMA)^{16}(PMMA/PS)^{16}$ 64-layer film created by simply folding a single 32-

layer PS/PMMA film (average layer thickness ~ 87 nm) to create a half-wavelength defect in the center of the quarter-wavelength stack.

Figure 1 shows data from an atomic force microscopy (AFM) scan across a micro-tomed multilayer slice for a 32-layer (PS/PMMA)¹⁶ sample of the type assembled for these measurements. Typical layer thickness variations for the process used to create these 32-layer and 128-layer films were the subject of study in Ref. [4] and [32]. The thickness distributions were found to have nominal standard deviations of 15% and 24%, respectively, but were not Gaussian.[32] As noted above, the materials used in this study were chosen for their amenability to co-extrusion processing and the quality of the reflection band, not for their inherent bulk Faraday rotation characteristics. Although the inherent Faraday effects in the constituent polymers of our system are several orders of magnitude smaller than those of more commonly studied iron-garnet materials, we are encouraged by recent reports of polymer materials showing anomalously large Faraday rotation comparable to those of ferromagnetic materials,[33,34] and by reports of the incorporation of high permeability materials into an amorphous matrix using disperse nanostructures.[35,36]

B. Faraday Rotation Measurement

Faraday rotation is typically measured by the transmitted light intensity change caused by the rotation of polarization through angle θ_F for light transmitted through the material in the direction of an applied magnetic field. We can express the Faraday rotation angle in terms of the light transmitted through a sample placed between a polarizer and analyzer in the presence of forward and backward magnetic fields, yielding,

$$\theta_F = -\frac{1}{2 \tan(\theta_{pol})} \times \frac{I_{B-field \ forward} - I_{B-field \ backward}}{I_{B-field \ forward} + I_{B-field \ backward}} \quad (2)$$

where θ_{pol} is the angle between the initial input polarizer just before the sample and the analyzer just after the sample, and B-field refers to the applied magnetic field. $I_{B\text{-field forward}}$ and $I_{B\text{-field backward}}$ are the light intensities when the magnetic field is parallel and anti-parallel to the light propagating direction, respectively, which are identical, of course, when $\theta_{pol} = 0$.

We see from Eq. (2) that the choice of angle θ_{pol} helps to determine the sensitivity of a Faraday rotation measurement, i.e., how small of a rotation angle can be measured. The intensity stability of the system ultimately limits the sensitivity of the Faraday rotation measurement. If $\theta_{pol} = 45^\circ$ (commonly used in other Faraday rotation measurement, e.g. see Refs. [14,37]), then $2 \tan(\theta_{pol}) \cong 2$ and a 1% variation in the light intensity corresponds to a maximum rotation angle resolution sensitivity of $\pm 0.3^\circ$. If, however, a larger angle is used (for example, $\theta_{pol} = 85^\circ$ as in most of our experiments), then $2 \tan(\theta_{pol}) = 22.8$ and the resolution is increased by a factor of 11.4. To make our sample measurements, we kept the analyzer usually at either 85° or 88° with respect to the polarizer, depending upon the amount of light transmitted through the sample. The stability of our setup allowed measured rotations as small as 0.002° with a resolution of 0.001° .

The experimental setup is shown in Fig. 2. Instead of measuring the change in light intensity arising from switching on and off the magnet (Varian V4000) (the magnet field for the 128-layer measurement was 1.04 ± 0.05 T, and the field for 64-layer measurement was 1.57 ± 0.05 T), we measured the difference in the signal between equal forward and backward longitudinal magnetic fields. Using equal forward and backward applied magnetic fields offers two advantages: (1) the amplitude of the resulting signal is doubled, and (2) quadratic artifacts caused by mechanical distortions in the strong magnetic field are eliminated, much as would be

the case with an ac detection system.[37] Within the limits of our system, however, we found that we were able to achieve larger magnetic fields and better resolution with dc magnetic fields applied alternately in the forward and backward directions (see Fig. 3 inset), and use of a digital intensity measurement based on TAOS TSL237 sensors.

Because of the small changes being measured, the intensity stability of the light source needed to be better than 0.1%. Rather than use a tunable laser source, which can easily exhibit noise at a few percent unless actively stabilized, we used a 20-W high-lumen broadband LED operating at a constant 25 A as the light source (PhlatLight CBT 120-G from Luminus Devices, Inc.[38]). This ice-water cooled LED exhibited a broad emission spectrum from 450 nm to 600 nm with an overall stability (for 100's of seconds) of the measured signal at the photodetectors of approximately 0.01%.

We used thin film polarizers on each side of our magnet coils and kept them as far as possible from the magnet poles (in our experiment, about 53 cm) without losing significant throughput. The sample was mounted on a non-magnetic holder between the two coils. A monochromator with a resolution of 2.5 nm was used to select the wavelength range incident on the detectors for each measurement. The relatively low resolution was necessitated by the low light levels present at the detector, especially when far from the LED's peak output or deep within the reflection band of our multilayers.

3. RESULTS

A. Faraday Rotation in Multilayers

As a check of our setup, we measured the Verdet coefficients of BK7 glass and of PMMA and PS monolith films. A 4.0-mm BK7 glass slab was measured at the conventional analyzer angle of $\theta_{pol} = 45^\circ$ because this thickness produced a relatively large polarization rotation compared to

the polymer monoliths and our multilayer sample. From our measurements, the Verdet constant was calculated to be $V = 8.0 \pm 0.1$ Rad/(T-m) at 491 nm, which agrees with the spectrally adjusted value in the literature for this wavelength.[39]

The thicknesses of the PMMA and PS monolith films were 220 μm and 208 μm , respectively. These films were characterized using an analyzer angle of $\theta_{pol} = 80^\circ$. Both the PMMA and PS monoliths were scanned from 450 nm to 600 nm and the measured Faraday rotation (Verdet) spectra are shown in Fig. 3. The inset on the top right of Fig. 3 shows an example of the experimental data we collected for forward and backward applied magnetic fields. At each wavelength, the light intensity was integrated for 150 seconds with the forward B-field and then 150 seconds with the backward B-field and each measurement was then repeated three times. Both the PS and PMMA Verdet spectra were fit using a modified Becquerel/Cauchy dispersion model $V = a/\lambda^2 + b/\lambda^4$ (c.f. Ref 40), where λ is the wavelength in meters and a and b are the fitting parameters, which are $a = 7.40 \times 10^5 \text{ m}^2\text{T}^{-1}$, $b = 1.10 \times 10^{11} \text{ m}^4\text{T}^{-1}$ for PMMA and $a = 2.27 \times 10^6 \text{ m}^2\text{T}^{-1}$, $b = 2.21 \times 10^{11} \text{ m}^4\text{T}^{-1}$ for PS. The experimental value of both PMMA and PS closely agree with literature values.[16,40]

We then measured a 128-layer PMMA/PS multilayer film which had been made by the co-extrusion method described above and in Ref. [32]. This multilayer film has a total thickness of about 11 μm , representing an interaction length for which a pure PMMA sample would show rotation of 0.0038° per Tesla at 500 nm. The transmission spectrum for our multilayer sample was measured using an Ocean Optics USB4000 Spectrometer, and the sample's reflection band was centered at 505 nm. The Faraday rotation spectrum was measured with the analyzer setting at $\theta_{pol} = 88^\circ$ with respect to the polarizer, and the rotation values were subsequently calibrated

based on the measured values at 491 nm with the analyzer setting at $\theta_{pol} = 85^\circ$. The Faraday rotation angles were also corrected by subtracting the small measured rotation angle without the sample present. This residual rotation, we believe, is caused by the Faraday effects of the remaining optical elements, as well as systematics due to hysteresis in our magnet. The results are shown as a function of incident wavelength in Fig. 4. Outside of the reflection band region, the experimental value for the multilayers is close to the average value for combined PMMA and PS monoliths of the same total thickness as our multilayers, which is reasonable because multilayer interference effects in the off-band range are weak. Inside the reflection band, the effective Verdet constant drops markedly. Near the left edge of the band, a clear peak shows an enhancement by a factor of about 1.5 which corresponds well to the location of the small, but significant defect in the reflection band centered at the same wavelength. On right edge, the enhancement is also present, but at a significantly lower level, consistent with the wide spectral averaging used and significant layer thickness variation present in this sample. We note that although it appears that the maximum enhancement is close to the value for a PS monolith of the same overall thickness (which is the constituent with the higher inherent Verdet constant), our modeling and additional measurements confirm that this is not a general result. With a multilayer system of higher uniformity and with a detection scheme of narrower wavelength spread, the Faraday rotation for the multilayer material exceeds the value for an equally-thick monolith of the higher Verdet material alone.

As a test of our rotation model at both reflection band-edge and band defects, we next measured a folded multilayer film configured as $(\text{PS/PMMA})^{16}(\text{PMMA/PS})^{16}$, as previously described. The measured results are shown in Fig. 5. As can be seen, the central transmission region splitting the reflection band corresponds to a region of enhanced effective Verdet 1.5

times that of a monolithic structure based on an average of the Verdet coefficients of the two constituent species. In this case, the edge-enhancement on the long wavelength side of the reflection band can also be seen, though reduced in size by spectral averaging and likely further reduced by the effects of layer thickness variations.

B. Application of Theory

Quantitatively complete versions of linear optical transport that include Faraday rotation commonly use a 4×4 transfer matrix formalism in which the off-diagonal matrix elements provide coupling between perpendicular polarization states[22,41] in each layer. Although this approach is wholly satisfactory as a quantitative method connecting the microstructure of the layered system to the overall optical properties, we suggest that it obscures the following simple physical narrative for the modulations of the magneto-optical rotation across the reflection stop band and at band defects.

An alternative approach highlights the utility of thinking of the transport in time rather than in space. This conceptually simpler approach uses only 2×2 transfer matrices (that is, transport of a single polarization), and yet elucidates quantitatively the connection between the reflection band structure and the Faraday rotation. To begin, we recast the bulk Verdet coefficients V per unit length L (of Eq. (1)) into reduced Verdet coefficients \tilde{v} per unit time t in the material. In practice, for bulk materials, we take $\tilde{v} = Vv_g$ where $v_g = \frac{\partial \omega}{\partial k}$ is the group velocity. In passing we note that recasting of Faraday rotation in terms of time is very natural from the point of view of quantum optics where the rotation angle is a convolution product of the magnetic field induced detunings (Zeeman effect, linear at small field) and the density of the transition-allowed states all multiplied by the time in the material. (See Ref.[42] for a popular review of this viewpoint; see also Ref.[43] for the range of validity of one of the approximations

used to get Eq.(1) from this viewpoint.) To determine the Faraday rotation caused by transport through any structure, one need only calculate the time spent in each species of the structure and multiply that species' Verdet (in time units). In a multilayer system, however, the time spent in each species is not a simple function of the thickness; the net effect of matching boundary conditions at each interface greatly influences the time. The derivation in the Appendix, for simplicity here for a two-component lattice multilayer maintains that

$$\frac{\theta_F}{B} = \sum_{\text{all layers}} V_{V_g} t_D = (V_{V_g})_A t_A + (V_{V_g})_B t_B = \tilde{V}_A t_A + \tilde{V}_B t_B, \quad (3)$$

where A and B indicate the two constituent species of the system (PMMA and PS in our systems), and t_A and t_B are the time spent in each species.

Before attempting to compute t_A and t_B , however, we first compute the total time spent

in the multilayer $t_D = t_A + t_B$ by appealing to the group velocity delay, $t_D = \frac{\lambda^2}{2\pi c} \frac{d\phi}{d\lambda} \approx \frac{\lambda^2}{2\pi c} \frac{\Delta\phi}{\Delta\lambda}$,

where ϕ is the phase of the transmitted electric field relative to the incoming electric field as a function of the wavelength λ . As with the multilayers' transmittance and reflectance, this phase ϕ and therefore t_D can be computed in a straightforward manner from the 2×2 transfer matrices of a single polarization[1] or can be determined experimentally. For any layer i within the stack, the total 2×2 transfer matrix can be split into three matrices such that $N_i M_i P_i$ where N_i and P_i represent the partial transfer matrices corresponding to the stack elements to the left and right, respectively, of the layer with 2×2 matrix M_i . The electric field $E_i(z)$ can then be calculated within the i^{th} layer at any point z within the layer as described in Ref. [44]. Although wave transport is dominated by evanescence at the deepest point of the reflection band, there is no

problem with computing t_D as defined above.[45] Also, it is worth remarking that what we are calling “total time” t_D is proportional to the local density of states in the multilayer.[46]

The most clear, simple physical way to apportion t_D into a time per species, t_A and t_B , is by reference to the probability of finding the photon in one species or the other. Note that we are determining, at steady state, the average time spent by a photon in each species’ layers, which is different than the time taken to get to each of those layers, a quantity that is apparently not well defined (see, for example, Refs. [45,47]). We show in the Appendix that the probability of finding a photon in one or the other species in a symmetrical stack is approximately proportional to the steady state field energy in that species. Relating the species-to-species relative field energy density to the time average of the presence of a photon in each species is an ergodic assumption about the light transport in these structures. Note that our method of using time delay in the multilayer system to predict Faraday rotation gives the exact same result as the 4×4 matrix method in the limit of a single high-Q Fabry-Perot cavity when ellipticity is taken into account.[48] The method is equally applicable to multi-layers with large index differences and with more well-defined reflection bands, but the model is expressly stated to be limited to situations in which a reasonable amount of structural symmetry is present. The limits of this approach are that it does not account for the difference in energy between the front and back ends of the stack due to the relative amounts of reflection and transmission at each wavelength.

Thus, we use standard 2×2 transfer matrix techniques to calculate the local energy density contours for our structures by dividing each layer into sublayers (ten in our case, though we have observed that further subdivision does not improve the fits for our systems) and summing the electric field energy density, $u_{A,B} = \sum (n^2 E^2)_{A,B}$, for each species over its sublayers.[44] As supported by the Appendix, these energy densities correspond to the

likelihood of finding a photon at each point in the stack and thus are used to find the time spent

in each constituent species as, for species A, $t_A = \frac{u_A t_D}{u_A + u_B}$. This time spent in each species is

then weighted by the species' bulk Verdet coefficient and the species' group velocity, (as

described earlier to get \tilde{v}), found from the index of refraction dispersion, $v_g = \frac{c}{n} \left(1 + \frac{\lambda}{n} \left(\frac{dn}{d\lambda} \right) \right)$.

Thus, the Faraday rotation per applied magnetic field for the entire multilayer stack is very nearly:

$$\frac{\theta_F}{B} = \tilde{v}_A t_A + \tilde{v}_B t_B = \frac{(V_{v_g})_A \sum_{A \text{ layers}} (nE)^2 + (V_{v_g})_B \sum_{B \text{ layers}} (nE)^2}{\sum_{\text{All layers}} (nE)^2} t_D. \quad (4)$$

As a test of the assumptions made in the derivation in the Appendix, we compare our results from Eq. (4) to the predictions from more standard 4×4 transfer matrix techniques for calculating Faraday effects in multilayers.[22] Our implementation of this 4×4 transfer matrix approach is consistent with those previously published by others for both the transmission and Faraday characteristics of purely dielectric multilayers starting from considerations of magnetically-induced circular birefringence, i.e., the differential indices of refraction for left circularly polarized (LCP) light and right circularly polarized (RCP) light in the presence of an applied magnetic field and, for small fields, linear in that field.[18,49]

To connect the results of our modeling to our experimental results, we start with the values for the bulk Verdet spectral dispersion formula obtained by fitting bulk Verdet constants reported elsewhere in the literature for PMMA[40] and PS[16]. The spectral dependence of the Verdet was approximated from the measurements described in Section 2 above. In our

calculation, we used the Cauchy refractive index dispersion, $n^2(\lambda) = n_{\lambda=\infty}^2 + \frac{c_1}{\lambda^2}$. In our case, the two parameters $(n_{\lambda=\infty}^2, c_1)$ correspond to $(2.40, 8.31 \times 10^4)$ for PMMA and $(2.61, 6.14 \times 10^4)$ for PS, respectively, with c_1 in nm^2 [50,51]. Using this approach, we calculated the transmission and Faraday rotation θ_F/B in our 128-layer and folded 64-layer PMMA/PS polymer.

The results of our modeling as a function of incident wavelength are shown in Fig. 6. For all of these graphs, we assumed zero variation in the individual layer thickness and a purely monochromatic probing light. There are no free parameters used in comparing the two approaches for determining the Faraday rotation.

Immediately apparent in the 128-layer case are the enhanced band edge effects and the suppressed rotation within the reflection band, consistent with our measured results shown in Fig. 4. In the folded 64-layer case, there is, in addition, an even greater enhancement at the reflection-band central defect caused by the half-wavelength defect in the quarter wavelength stack, consistent with our measured results shown in Fig. 5. Although one might expect that even the low levels of light transmitted in the reflection band would experience at least the rotation expected for a pair of monoliths of the same total thickness, simulation and experiment show that this is not the case. This somewhat unexpected *suppression* of Faraday rotation seen in the stop band can be understood primarily as a consequence of the *reduced* time spent in the material as the group velocity of the waves in the reflection band is greater than the group velocity near the band edge or even well outside the reflection band.

Qualitatively, the measured results shown in Fig. 4 and the simulated results shown in Figure 6(b) for the case of 128 layers differ primarily due to the effects of layer thickness variations and spectral averaging. We consider these effects explicitly in the calculated results

shown in Fig. 7 based on an assumed variation in layer thickness comparable to that shown in Fig. 1 and the use of probing light of a finite spectral width. Again, both the standard 4×4 transfer matrix simulations and the predictions based on the time-reduced Verdet values for each species and the effects of the multilayer structures on the group velocity delay yield almost identical results. In this case, as in Fig. 4, the transmission band can be seen to be lossier and wider overall, yet with complicating features, such as the increase in transparency at just below 500 nm. This feature can be understood to be a defect in the reflection band arising from broken symmetry in the quarter-wavelength stack caused by layer thickness variations. In this instance, in addition to a smaller edge enhancement in the predicted Faraday rotation of the stack, we note an additional enhancement in the rotation at the location of this defect in the reflection band. Moreover, by changing the random thickness variations, we found that the band-defect enhancement shifted to the opposite side of the band as compared to the exact result for perfectly even layers, leading to the anomalous high-energy band-edge enhancement seen in both Figs. 4 and 7.

Note that the results of Figs. 6(b) and 6(d) and Fig. 7 include the effects of ellipticity in the output polarization angle as predicted by Eq. (A3), but do not indicate the degree of ellipticity directly, which we did not measure. Figure 8(a) shows that, away from the reflection band, the ellipticity is very small and both the 4×4 and 2×2 transfer matrix methods yield essentially the same results. In the reflection band, however, the two simulations diverge due to the accumulated effects of differential reflectivities increasing the ellipticity of the output. Note that our 2×2 transfer matrix approach does not take into account the magnetic-field induced difference in the reflectivities for the two polarization directions at each layer interface which leads to an elliptically polarized output, yet it is in closer agreement with the 4×4 transfer

matrix method that includes the effects of ellipticity using Eq. (A3) than one that does not. We believe that much of the remaining discrepancy between the results of the 2×2 and 4×4 transfer matrix approaches can be explained in terms of the ellipticity of the output polarization. In Fig. 8(b) we plot the difference between the models used in Fig. 6(d) ($\theta_{F_{2 \times 2}} - \theta_{F_{4 \times 4}}$). As can be seen, this difference closely tracks the predicted ellipticity.

In this Section and the Appendix, we have described our experimental results and an alternative way to quantitatively understand the Faraday rotation in lattice structures in terms of the time spent in the various species making up the structure. Admittedly, this alternate approach still requires significant computation, but we maintain that this approach quantitatively delineates the role of the constituent magneto-optical rotary powers of the member species, and, separately, the dispersion caused by the multilayer in causing the modulations of the Faraday rotation. It is hoped that such a simple physical narrative may be helpful to those designing composite structures with larger Verdet materials than we studied, and that it may suggest ways to understand other transport related phenomena in complex media.

4. CONCLUSION

Light at wavelengths well outside the reflection band will travel essentially once through the system and thus the Faraday rotation is on average the species weighted rotation of the constituent bulk materials. Light at wavelengths near the reflection band edge or at band-defects, however, experiences multiple reflections when passing through the multilayer film, effectively increasing the time of transit through the film and proportionally increasing the rotation angle. Our experiments show that band-defect enhancements in samples with random layer thickness variations can be controlled somewhat when systematic defects are included in the structure through, for example, the use of folded multilayers. We believe that all cases can be explained

by changes in the group velocity associated with band-edges and band-defects and that the group velocity delay scales appropriately with the Faraday rotation for these systems, and not naively with thickness. Our experimental results are consistent with our model which shows that the Faraday rotation per applied B-field in symmetrical multilayer stacks is just the time in each constituent material scaled by the Verdet in that material written in time units. Furthermore, the time in each material can be estimated by the weighting the total time delay by the proportionate amount of electromagnetic energy density in that material. .

Further work is also ongoing to enhance the Faraday effect in these systems by incorporating magnetically active materials into the layered stacks. In addition, we are exploring the use of systematically prepared defects and gradient multilayer structures in order to further enhance the Faraday rotation.

To summarize, we modeled and measured the magneto-optic rotation caused by the Faraday effect in layered polymer films composed of alternating layers of PMMA and PS produced through a single step co-extrusion process. Our simple conceptual model quantitatively captures band-edge and band-defect enhancements of the Faraday rotation and the significant drop in the Faraday rotation in the center of the reflection band. Our experimental setup for measuring Faraday rotation is capable of 0.001° resolution down to around 0.002° rotation and our measurements show band-defect enhancements and edge enhancements in a manner consistent with the group velocity delays of light propagating through the system.

ACKNOWLEDGEMENTS

This work is supported by the National Science Foundation under Grant No. DMR 0423914. Youngstown State University acknowledges the contribution of the State of Ohio, Department of Development, State of Ohio, the Chancellor of the Board of Regents and Third Frontier

Commission, which provided funding in support of the Research Cluster on Surfaces in Advanced Materials.

APPENDIX

The starting point for deriving our assertion Eq.(3) is the standard (4×4 transfer matrix) technique for calculating Faraday effects in multilayers.[22] Our implementation of this the 4×4 transfer matrix approach is consistent with those previously published by others for both the transmission and Faraday characteristics of purely dielectric multilayers starting from considerations of magnetically-induced circular birefringence, i.e., the differential indices of refraction for left circularly polarized (LCP) light and right circularly polarized (RCP) light in the presence of an applied magnetic field and, for small fields, linear in that field.[18,52] Operationally, by “time spent in each component of the medium” we denote the energy-weighted group velocity delay in each component. Various parts of this correspondence have been noted in the literature, but this derivation delineates those parts of the correspondence that are always true from those appear to depend on the particulars of our systems (parity symmetry) and approximation.

Note that at zero magnetic field, the orthogonal linear polarization states E_x, E_y moving through this non-birefringent material have identical characteristic 2×2 transfer matrices in the (E, H) basis of the usual form for multilayer transmission calculations,

$$\mathbf{M} = \begin{pmatrix} \cos \delta & i/\eta \sin \delta \\ i\eta \sin \delta & \cos \delta \end{pmatrix} \quad (\text{A1})$$

with η the complex impedance of the medium at frequency ω , and $\delta = nk_0x$ is the optical path length measured in vacuum wavelengths of the material in terms of the index of refraction, n , and the vacuum wavevector, k_0 . To couple these orthogonal polarization states, we combine the characteristic \mathbf{M} matrices for each layer with the 2×2 coupling matrices \mathbf{C} into a 4×4 transfer matrix $\mathcal{M} = \begin{pmatrix} \mathbf{M} & \mathbf{C} \\ -\mathbf{C} & \mathbf{M} \end{pmatrix}$ where the \mathbf{C} matrix parameterizes the vertical and horizontal optical rotation for the case of azimuthal symmetry (longitudinal applied magnetic field) assuming no absorption ($\eta = n$) or incoherent scattering. For purely dielectric materials, it can be shown that, in the limit of small Faraday rotations, \mathbf{C} takes the form

$$\mathbf{C} = VB \begin{pmatrix} -i \sin \delta & \left(\frac{1}{n}\right) \left(\cos \delta - \frac{\sin \delta}{\delta} \right) \\ n \left(\cos \delta + \frac{\sin \delta}{\delta} \right) & -i \sin \delta \end{pmatrix} \text{ where } VB \text{ is the product of the bulk Verdet}$$

coefficient for the constituent material, and the applied magnetic field ($\sim 1\text{T}$ for our experiments and simulations).[53] Note that in this limit $\mathbf{C} = \mathbf{C}_p + \mathbf{C}_s$ where we call the ‘‘primary’’ part \mathbf{C}_p of

the rotation is $\mathbf{C}_p = VB \begin{pmatrix} -i \sin \delta & \cos \delta / n \\ n \cos \delta & -i \sin \delta \end{pmatrix}$ and the ‘‘secondary’’ part \mathbf{C}_s is

$$\mathbf{C}_s = VB \frac{\sin \delta}{\delta} \begin{pmatrix} 0 & -1/n \\ n & 0 \end{pmatrix}. \text{ The characteristic } 4 \times 4 \text{ transfer matrix for each layer thus expresses}$$

the phase and amplitude changes in that layer (and interface) as well as the coupling of the LCP and RCP refractive indices as a function of applied magnetic field for the constituent materials. Operation of the transfer matrices \mathcal{M} of each layer on the fields expressed as a 4-dimensional

complex vector $\begin{pmatrix} E_x \\ H_y \\ E_y \\ -H_x \end{pmatrix}$ (where, in our case, the incoming E_y, H_x are assumed to be zero), we

arrive at the (complex) values of the horizontal (E_x) and vertical (E_y) polarization output and

their ratio $\chi = E_x/E_y$.

The fact that C_p and C_s scale differently with the thickness of the layers indicates that in most situations of interest here, the Faraday rotation is dominated by the contributions from the primary part C_p , which we will henceforth denote simply C . Note that

$$\mathbf{M}^{-1}\mathbf{C} = VB \begin{pmatrix} 0 & 1/n \\ n & 0 \end{pmatrix} = iVB \{ \partial_\delta \mathbf{M} \} \mathbf{M}^{-1}$$

where to get the last equality we have ignored the

dispersion in the n (we ignore the material's intrinsic refractive index dispersion throughout this appendix).

The optical transport in the complex medium is the product of the 4×4 transfer matrices \mathcal{M} for each component labeled by ' i ' in sequence. In the limit of small Faraday rotations, we

need only keep terms linear in the V_i and thus have $\mathcal{M} = \prod_i \mathcal{M}_i = \begin{pmatrix} \mathbf{M} & \mathbf{C} \\ -\mathbf{C} & \mathbf{M} \end{pmatrix}$ where now

$$\mathbf{M} = \prod_i \mathbf{M}_i \text{ and the } \mathbf{C} = \mathbf{M}\mathbf{S} \text{ where } \mathbf{S} = \sum_i \mathbf{P}_i^{-1} \mathbf{M}_i^{-1} \mathbf{C}_i \mathbf{P}_i \text{ where we take } \mathbf{M} = \mathbf{N}_i \mathbf{M}_i \mathbf{P}_i \text{ for each } i$$

where $\mathbf{N}_i = \prod_{j>i} \mathbf{M}_j$, and $\mathbf{P}_i = \prod_{j<i} \mathbf{M}_j$.

The vectors $\mathbf{w}_t = \frac{1}{\sqrt{2}}(1,1)$ and $\mathbf{w}_r = \frac{1}{\sqrt{2}}(-1,1)$ are the transmission and reflection

propagation eigenstates in the $n=1$ medium to the left and right of the layered medium. Thus,

taking the ratio of the horizontal transmitted component to the vertical transmitted component,

$$\text{the observed rotation is } \theta_F \sim \arctan(\chi) \sim \left| \mathbf{w}_t^\dagger \mathbf{M} \mathbf{S} \mathbf{M}^{-1} \mathbf{w}_t \right| = \left| iB \sum_i V_i \mathbf{w}_t^\dagger \mathbf{N}_{i+1} \{ \partial_\delta \mathbf{M}_i \} \mathbf{M}_i^{-1} \mathbf{N}_{i+1}^{-1} \mathbf{w}_t \right|$$

We can now relate this expression to sum of the energy-weighted time in each layer multiplied by the rotation (per unit time) in that layer. Note the transmission amplitude is

$$\tau = \frac{1}{\mathbf{w}_t^\dagger \mathbf{M}^{-1} \mathbf{w}_t}. \text{ One observable from this transmission amplitude is the total group velocity}$$

delay across the entire multilayer; it is “ i ” times the derivative with respect to the wavevector of the phase of the transmission amplitude,

$$\partial_{k_0} \phi = \frac{1}{2i} \left[\frac{\partial_{k_0} \tau}{\tau} - \frac{\partial_{k_0} \tau^*}{\tau^*} \right] = \frac{\tau^2}{2i} \left[\mathbf{w}_t^\dagger \left(\partial_{k_0} \mathbf{M}^{*-1} \right) \mathbf{w}_t \mathbf{w}_t^\dagger \mathbf{M}^{-1} \mathbf{w}_t - c.c. \right]$$

Now we use the fact that the multilayer systems we are studying are typically very close to being parity symmetric, that is, $\mathbf{M}^{-1} = \mathbf{T} \mathbf{M} \mathbf{T}$ where $\mathbf{T} = \begin{pmatrix} -1 & 0 \\ 0 & 1 \end{pmatrix}$ maps outgoing states to ingoing states (under time and parity reversal) in the original 2x2 scattering basis. Further, in the limit that there is no absorption (implying that the power quadratic form \mathbf{P} satisfies $\mathbf{P} = \mathbf{M}^\dagger \mathbf{P} \mathbf{M}$ where in this 2×2 basis $\mathbf{P} = \begin{pmatrix} 0 & 1 \\ 1 & 0 \end{pmatrix}$), this reflection symmetry of the film implies that $\mathbf{M}^{-1} = \mathbf{M}^*$. We reiterate that this is strictly speaking only true for the multilayers $(AB)^N (BA)^N$ or $(AB)^N A$, in the notation of this paper but that $(AB)^N$ for large N is, in a sense, close to being parity symmetric.

Under the even parity/no absorption assumptions, the $\mathbf{w}_r \mathbf{M}^{-1} \mathbf{w}_t$ is purely imaginary.

Then, using completeness, $\mathbf{w}_t \mathbf{w}_t^\dagger + \mathbf{w}_r \mathbf{w}_r^\dagger = \begin{pmatrix} 1 & 0 \\ 0 & 1 \end{pmatrix}$, the total group velocity delay takes on a very

simple form: $\partial_{k_0} \phi = -i\tau^2 \mathbf{w}_t^\dagger (\partial_{k_0} \mathbf{M}) \mathbf{M}^{-1} \mathbf{w}_t$ and note that the expression $\mathbf{w}_t^\dagger (\partial_{k_0} \mathbf{M}) \mathbf{M}^{-1} \mathbf{w}_t = \sum_j \mathbf{w}_t^\dagger N_j n_j l_j (\partial_\delta \mathbf{M}_j) \mathbf{M}_j^{-1} N_j^{-1} \mathbf{w}_t$, where n_j is again the index of refraction of the j^{th} layer and l_j is the thickness of that layer.

The $N_j^{-1} \tau \mathbf{w}_t$ is the local (E_j, H_j) at that layer's output facet. The $n_j (\partial_\delta \mathbf{M}_j) \mathbf{M}_j^{-1}$ as a quadratic form on that field vector gives one the normalized local energy density in the standing wave and scaled by l_j gives the normalized local circulating energy in the j^{th} component.

Explicitly, let $N_j = \begin{pmatrix} a & ib \\ ic & d \end{pmatrix}$ where by the non-absorption assumption a, b, c, d are real and because (steady state) transport is power conserving and preserves the bracket, $\det(N_j) = 1$.

Then $E_j = \tau(d - ib)$ and $H_j = \tau(a - ic)$ and the

$\mathbf{w}_t^\dagger N_j n_j l_j (\partial_\delta \mathbf{M}_j) \mathbf{M}_j^{-1} N_j^{-1} \mathbf{w}_t = n E_j^* E_j + \frac{1}{n} H_j^* H_j$. Note further that this energy density is constant

inside the j^{th} component, as follows because $\begin{pmatrix} n^2 & 0 \\ 0 & 1 \end{pmatrix}$, the quadratic form for the local energy

density, commutes with the infinitesimal version of Eq.(A1) above. That is, as expected in steady state, the standing wave power density is spatially constant in each component.

At this point the connection between the group velocity delay $\partial_{k_0} \phi$ and the Faraday rotation θ_F is straightforward. The derivative $\partial_{k_0} \phi$ is related to the terms making up the Faraday rotation by apportioning the total delay $t_d = \frac{1}{c} \partial_{k_0} \phi$ into delays in each component proportional to the total energy density in that component. For simplicity of notation, assume that the system was just $(AB)^N$. Then $t_A = \langle u_A \rangle t_d$ is the time in material A and $t_B = \langle u_B \rangle t_d$ where “ $\langle \rangle$ ” means

normalized in terms total circulating energy $u_A + u_B$ in this case. Thus, for the primary part of the Faraday rotation, $\frac{\theta_F}{B} = \tilde{U}_A t_A + \tilde{U}_B t_B$, as described in Eq.(3).

In summary, we have derived a connection between the primary part of the Faraday rotation (usually computed in the 4×4 formalism) and the total group delay in a complex linear medium (from the 2×2 problem), assuming no intrinsic media dispersion, no absorption and parity of the medium. We have shown that the local energy of a layer (again, using the 2×2 formalism) is a proxy for what fraction of the delay is spent in that layer. This furnishes a rather complete analytical description of the Faraday rotation in complex media in terms of the rotary power of the individual components and the dispersion created by the multilayer structure itself.

Note that in conventional Faraday measurement, the Faraday rotation angle is calculated assuming linearly polarized light input and output (E_x) which neglects ellipticity. $\theta_F = \tan^{-1}(\chi)$. In a 1D-PC system, the ellipticity accumulated through multiple reflections can be significant, however, due to the difference between the RCP and LCP refractive indices in each layer. In particular, near and in the reflection band, the ellipticity of the output light is indicated by χ being complex. In general the relationship between the azimuth angle θ and ellipticity angle ϵ for the real and imaginary parts of the output field ratios is then given as[54]

$$\text{Re}(\chi) = \frac{\tan \theta (1 - \tan^2 \epsilon)}{1 + \tan^2 \theta \tan^2 \epsilon}, \quad \text{Im}(\chi) = \frac{\tan \epsilon (1 + \tan^2 \theta)}{1 + \tan^2 \theta \tan^2 \epsilon}. \quad (\text{A2})$$

If we assume the input azimuth angle is zero (linear polarization in \hat{x}), the transmitted Faraday rotation angle and the ellipticity angle can be finally written as

$$\text{Faraday: } \theta_F = \frac{1}{2} \tan^{-1} \left(\frac{2 \text{Re}(\chi)}{1 - |\chi|^2} \right), \quad \text{Ellipticity: } \epsilon = \frac{1}{2} \sin^{-1} \left(\frac{2 \text{Im}(\chi)}{1 + |\chi|^2} \right). \quad (\text{A3})$$

The values for the Verdet coupling of the LCP and RCP refractive indices as a function of magnetic field used in the parameter V for each constituent species were directly calculated from Verdet spectral dispersion formula obtained by fitting bulk Verdet constants reported elsewhere in the literature for PMMA[40] and PS[16].

Figure Captions

Figure 1. (a) AFM image of a cross-section of a typical 32-layer PMMA/PS co-extruded film. (b) Layer thickness distribution for the film above determined by AFM analysis. The average thickness of the PMMA and PS layers in this case was found to be, respectively, 80 nm and 92 nm.

Figure 2. Schematic setup of our Faraday rotation experiment. LED: high-lumen green LED, L1: collimation lens, P1: thin film polarizer, BS: beam splitter, P2: thin film polarizer/analyzer mounted on rotary mount, M1 & M2: mirrors, Mono: monochromator, OO: Ocean Optics CCD.

Figure 3. (color online) Verdet constant spectral measurements for monoliths of PS (solid red circles) and PMMA (open blue circles). The inset shows typical data from our intensity-to-frequency detectors during applied magnetic field reversals.

Figure 4. (color online) Measured spectral transmission (solid black circles) and effective Faraday rotation per Tesla (open red circles) of the 128-layer PMMA/PS multilayer film as a function of the incident wavelength.

Figure 5. (color online) Measured spectral transmission (solid black circles) and effective Faraday rotation per Tesla (open red circles) for a 64-layer folded $(\text{PS/PMMA})^{16}(\text{PMMA/PS})^{16}$ multilayer film as a function of the incident wavelength.

Figure 6. (color online) (a), (b) Simulation of 128-layer film of PMMA/PS multilayer; (c), (d) simulation of a folded 64-layer film. (a) and (c) show the predicted transmission spectra from the multilayer stack. (c) and (d) show the predicted effective Verdet spectra using both the standard 4×4 matrix approach and the reduced Verdet, time-delay 2×2 transfer matrix approach described here. The bracketing red and blue lines show the predicted rotation from monoliths of PS and PMMA, respectively, of the same thickness.

Figure 7. (color online) Simulation of 128 layer of PMMA/PS multilayer with layer thickness of 87nm, but with probing light has a finite Gaussian spectrum width of from 3.5 to 4.5 nm and a layer thickness variation of 10%. The solid line shows the predicted transmission spectrum and the dashed and dotted red lines shows the predicted Faraday rotations using the reduced Verdet, time-delay 2×2 transfer matrix approach and the standard 4×4 matrix approach, respectively.

Figure 8. (a) Comparison between predicted Faraday rotation for a folded 64-layer structure considering ellipticity (solid line), without considering ellipticity (dashed line), and using our time-based Verdet model (dotted line). (b) Comparison between the predicted ellipticity angle for this folded 64-layer case (solid line) and the scaled difference between the 4×4 and 2×2 transfer matrix results shown in Fig. 6(d) (dotted line).

REFERENCES

1. P. Yeh, *Optical Waves in Layered Media*, Wiley-Interscience, New Jersey (2005).
2. C.D. Mueller, S. Nazarenko, T. Ebeling, T.L. Schuman, A. Hiltner, and E. Baer, "Novel structures by microlayer coextrusion," *Polymer Eng. and Sci.* **37**, 355-362 (1997).
3. A.C. Edrington, A.M. Urbas, P. DeRege, C.X. Chen, T.M. Swager, N. Hadjichristidis, M. Xenidou, L.J. Fetters, J.D. Joannopoulos, Y. Fin, and E.L. Thomas, "Polymer-based photonic crystals," *Adv. Mater.* **13**, 421-425 (2001).
4. T. Kazmierczak, H. Song, A. Hiltner, and E. Baer, "Polymeric one-dimensional photonic crystals by continuous coextrusion," *Macromol. Rapid Commun.* **28**, 2210-2216 (2007).
5. M. Ponting, T.M. Burt, L.T.J. Korley, J. Andrews, A. Hiltner, and E. Baer, "Gradient Multilayer Films by Forced Assembly Coextrusion," *Industrial & Engineering Chemistry Research* **49**, 12111–12118 (2010).
6. C. Kallinger, M. Hilmer, A. Haugeneder, M. Perner, W. Spirkl, U. Lemmer, J. Feldmann, U. Scherf, K. Mullen, A. Gombert, and V. Wittwer, "A flexible conjugated polymer laser," *Adv. Mater.* **10**, 920-923 (1998).
7. S.Y. Chou, P.R. Krauss, and P.J. Renstrom, "Imprint of sub-25 nm vias and trenches in polymers," *Appl. Phys. Lett.* **67**, 3114-3116 (1995).
8. A. Roger, M. Meier, A. Dodabalapur, E.J. Laskowski, and M.A. Capuzzo, "Distributed feedback ridge waveguide lasers fabricated by nanoscale printing and molding on nonplanar substrates," *Appl. Phys. Lett.* **64**, 3257-3259 (1999).
9. G. Khanarian, M.A. Mortazavi, and A.J. East, "Phase-matched second-harmonic generation from free-standing periodically stacked polymer films," *Appl. Phys. Lett.* **63**, 1462-1464 (1993).

-
10. S. Fan, M. F. Yanik, Z. Wang, S. Sandhu, and M.L. Povinelli, “Advances in theory of photonic crystals,” *J. Lightwave Tech.* **24**, 4493-4501 (2006).
 11. H. Song, K.D. Singer, J. Lott, J. Zhou, J.H. Andrews, E. Baer, A. Hiltner, and C. Weder, “Continuous Melt Processing of All-Polymer Distributed Feedback Lasers,” *J. Mater.Chem.* **19**, 7520–7524 (2009).
 12. R. Katouf , T. Komikado, M. Itoh, T. Yatagai, S. Umegaki, “Ultra-fast optical switches using 1D polymeric photonic crystals,” *Photonics and Nanostructures – Fundamentals and Applications* **3**, 116–119 (2005) .
 13. Cf. V. Gasparian, M. Ortuno, J. Ruiz, and E. Cuevas, “Faraday rotation and complex-valued traversal time for classical light waves,” *Phys. Rev. Lett.* **75**, 2312-2315 (1995).
 14. P.R. Camp and R.C. Raymond, “A Photoelectric Polarimeter for Measurement of Transient Rotations,” *J. Opt. Soc. Am.* **42**, 237- 240 (1952).
 15. E.H. Hwang and B.Y. Kim, “Pulsed high magnetic field sensor using polymethyl methacrylate,” *Meas. Sci. Technol.* **17**, 2015-2021 (2006).
 16. S. Muto, N. Seki, T. Suzuki, and T. Tsukamoto, “Plastic Fiber Optical Isolator an Current Sensor,” *Jpn. J. Appl. Phys.* **31**, 346-348 (1992).
 17. M. Inoue, R. Fujikawa, A. Baryshev, A. Khanikaev, P.B. Lim, H. Uchida, O. Aktsipetrov, A. Fedyanin, T. Murzina, and A. Granovsky, “Magnetophotonic crystals,” *J. Phys. D: Appl. Phys.* **39**, R151-R161 (2006).
 18. M.J. Steel, M. Levy, and R.M. Osgood, “Large magneto-optical Kerr rotation with high reflectivity from photonic bandgap structures with defects,” and “ Photonic bandgaps with defects and the enhancement of Faraday rotation,” *J. Lightwave Tech.* **18**, 1289-1296 and 1297-1308 (2000).

-
19. I. Abdulhalim, "Analytic propagation matrix method for anisotropic magneto-optic layered media," *J. Opt. A: Pure Appl. Opt.* **2**, 557-564 (2000).
 20. S. Visnovsky, K. Postava, and T. Yamaguchi, "Magneto-optic polar Kerr and Faraday effects in periodic multilayers," *Opt. Express* **9**, 158-171 (2001).
 21. S. Visnovsky, R. Lopusnik, M. Bauer, J. Bok, J. Fassbender, and B. Hillebrands, "Magneto-optic ellipsometry in multilayers at arbitrary magnetization," *Opt. Express* **9**, 121-135 (2001).
 22. H. Kato, T. Matsushita, A. Takayama, M. Egawa, K. Nishimura, and M. Inoue, "Theoretical analysis of optical and magneto-optical properties of one-dimensional magnetophotonic crystals," *J. Appl. Phys.* **93**, 3906-3911 (2003).
 23. H.Y. Ling, "Theoretical investigation of transmission through a Faraday-active Fabry-Perot etalon," *J. Opt. Soc. Am. A* **11**, 754-758 (1994).
 24. M. Inoue, K. Arai, T. Fujii, and M. Abe, "Magneto-optical properties of one-dimensional photonic crystals composed of magnetic and dielectric layers," *J. Appl. Phys.* **83**, 6768-6770 (1998).
 25. S. Sakaguchi and N. Sugimoto, "Transmission Properties of Multilayer Films Composed of Magneto-Optical and Dielectric Materials," *J. Lightwave Technol.* **17**, 1087-1092 (1999).
 26. B. Wu, F. Lui, S. Lui, and W. Huang, "Research on transmission spectra of one-dimensional magneto-photonic crystals," *Optoelectron. Lett.* **5**, 268-272 (2009).
 27. M.J. Steel, M. Levy, and R.M. Osgood, "High transmission enhanced Faraday rotation in one-dimensional photonic crystals with defects," *IEEE Photonics Technol. Lett.* **12**, 1171-1173 (2000).

-
28. V.I. Belotelov and A.K. Zvezdin, "Magneto-optical properties of photonic crystals," *J. Opt. Soc. Am. B* **22**, 286-292 (2005).
29. S. Kahl and A.M. Grishin, "Enhanced Faraday rotation in all-garnet magneto-optical photonic crystal," *Appl. Phys. Lett.* **84**, 1438-1440 (2004).
30. S.I. Khartsev and A.M. Grishin, "[Bi₃Fe₅O₁₂/Gd₃Ga₅O₁₂]_m magneto-optical photonic crystals," *Appl. Phys. Lett.* **87**, 122504 (2005).
31. T.E. Bernal-Lara, A. Ranade, A. Hiltner, E. Baer, "Nano- and microlayered polymers: Structure and Properties," in *Mechanical Properties of Polymers Based on Nanostructure*, 1st ed., G.H. Micheler, F. Balta-Callaja, Eds., CRC Press, Boca Raton, FL 2005.
32. H. Song, K. Singer, Y. Wu, J. Zhou, J. Lott, J. Andrews, A. Hiltner, E. Baer, C. Weder, R. Bunch, R. Lepkowitz, and G. Beadie, "Layered Polymeric Optical Systems Using Continuous Coextrusion," *Proc. SPIE* **7467**, 74670A Nanophotonics and Macrophotonics for Space Environments III, E.W. Taylor; D. A. Cardimona, Eds. (2009).
33. G. Koeckelberghs, M. Vangheluwe, K. Van Doorselaere, E. Robijns, A. Persoons, and T. Verbiest, "Regioregularity in Poly(3-alkoxythiophene)s: Effects on the Faraday Rotation and Polymerization Mechanism," *Macromol. Rapid Commun.* **27**, 1920-1922 (2006). P. Gangopadhyay, R. Voorakaranam, A. Lopez-Santiago, S. Foerier, J. Thomas, R. A. Norwood, A. Persoons, and N. Peyghambarian, "Faraday Rotation Measurements on Thin Films of Regioregular Alkyl-Substituted Polythiophene Derivatives," *J. Phys. Chem. C* **112**, 8032-8037(2008).
34. F. Araoka, M. Abe, T. Yamamoto, and H. Takezoe, "Large Faraday Rotation in a π -Conjugated Poly(arylene ethynylene) Thin Film," *Appl. Phys. Express* **2**, 011501-011503 (2009).

-
35. M. Domínguez, D. Ortega, J.S. Garitaonandía, R. Litrán, C. Barrera-Solano, E. Blanco, M. Ramírez-del-Solar, Magneto-optic Faraday effect in maghemite nanoparticles/silica matrix nanocomposites prepared by the Sol–Gel method, *J. Magnetism Magnetic Mat.*, **320**, e725-e729 (2008).
36. K.E. Gonsalves, G. Carlson, M. Benaissa, M. Jose-Yacama´ D.Y. Kim and J. Kumar, “Magneto-optical properties of nanostructured iron,” *J. Mater. Chem.* **7(5)**, 703–704 (1997).
37. V.K. Valev, J. Wouters, and T. Verbiest, “Differential detection for measurements of Faraday rotation by means of ac magnetic fields,” *Euro. J. Phys.* **29**, 1099-1104 (2008).
38. See www.luminus.com.
39. M.J. Weber, Ed., *Handbook of Optical Materials*, pp. 259, 299 (CRC Press, 2003).
40. H.C.Y. Yu, M.A. van Eijkelenborg, S.G. Leon-Saval, A. Argyros, and G.W. Barton, “Enhanced magneto-optical effect in cobalt nanoparticle-doped optical fiber,” *Appl. Opt.* **47**, 6497-6501 (2008).
41. K.R. Heim and M.R. Scheinfein, “An alternative approach for magneto-optic calculations involving layered media,” *J. Magn Magn. Mater.* **154**, 141-152 (1996).
42. D. Budker, W. Gawlik, D.F. Kimball, S. F. Rochester, V.V. Yashchuk, A. Weiss, “Resonant nonlinear magneto-optical effects in atoms”, *Rev. Mod. Phys.* **74**, 1153-1201 (2002).
43. P. Berman, “Optical Faraday Rotation,” *Am. J. Phys.* **78**, 270-276 (2010).
44. L.A.A. Pettersson, L.S. Roman, and O. Inganas, “Modeling photocurrent action spectra of photovoltaic devices based on organic thin films,” *J. Appl. Phys.* **86**, 487-496 (1999).
45. See, e.g., H.G. Winful, “Tunneling time, the Hartman effect, and superluminality: A proposed resolution of an old paradox,” *Phys. Reports* **436**, 1–69 (2006); P.C.W. Davies, “Quantum Tunneling time,” *Am. J. Phys.* **73**, 23-27 (2005); and A.M. Steinberg, “How much

-
- time does a tunneling particle spend in the barrier region?” *Phys. Rev. Lett.* **74**, 2405–2409 (1995).
46. The reason we do not think that density of states concepts are as useful here is that the connection between time and the density of states is only direct in one dimension, whereas Eq. (3) we are claiming is general. Furthermore, it is not clear how to apportion the density of states to each constituent material as implied by t_A and t_B .
47. F.E. Low and P.F. Mende, “A Note on the Tunneling Time Problem,” *Annals of Physics* **210**, 380-387 (1991).
48. V. Gasparian, M. Ortuño, J. Ruiz, E. Cuevas, “Faraday Rotation and Complex Valued Traversal Time for Classical Light Waves,” *Phys. Rev. Lett.* **75**, 2312-2315 (1995).
49. S. Visnovsky, *Optics in Magnetic Multilayers and Nanostructures*, Series on Optical Science and Engineering, (CRC Press, Boca Raton, FL, 2006)
50. S.E. Caudill and W.T. Grubbs, “Interferometric Measurements of Refractive Index Dispersion in Polymers over the Visible and Near-Infrared Spectral Range,” *J. Appl. Polymer Science* **100**, 65-72 (2006).
51. I.D. Nikolov and C.D. Ivanov, “Optical plastic refractive measurements in the visible and the near-infrared regions,” *Appl. Opt.* **39**, 2067-2070 (2000).
52. S. Visnovsky, *Optics in Magnetic Multilayers and Nanostructures*, Series on Optical Science and Engineering, (CRC Press, Boca Raton, FL, 2006)
53. Cf. C. Koerdt, *Magneto-Spatial Dispersion Phenomena: Photonic Band Gaps and Chirality in Magneto-Optics*, PhD Thesis, University of Konstanz (2004) Found online <https://docs.google.com/viewer?url=http://www.ub.uni-konstanz.de/kops/volltexte/2004/1376/pdf/thesis-kops.pdf&pli=1>

-
54. R.M.A. Azzam and N.M. Bashara, *Ellipsometry and Polarized Light*, North-Holland Pub. Co. (1977).

Figure 1.

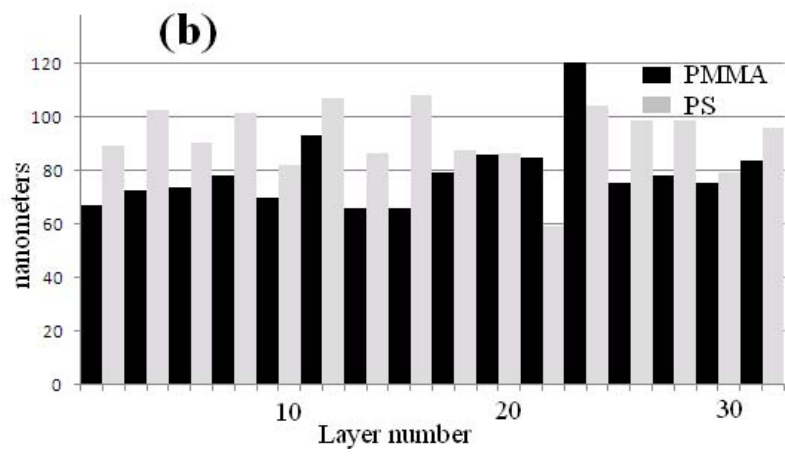
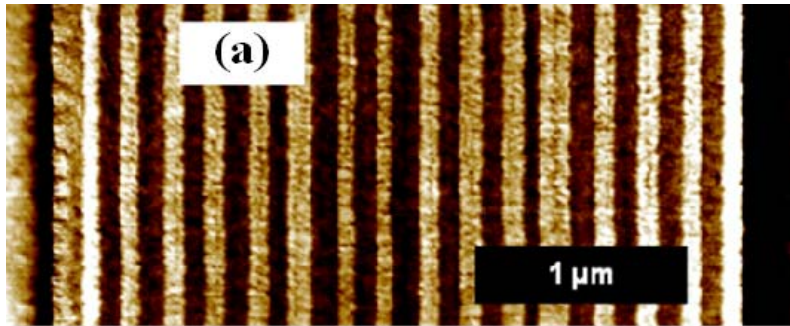


Figure 2.

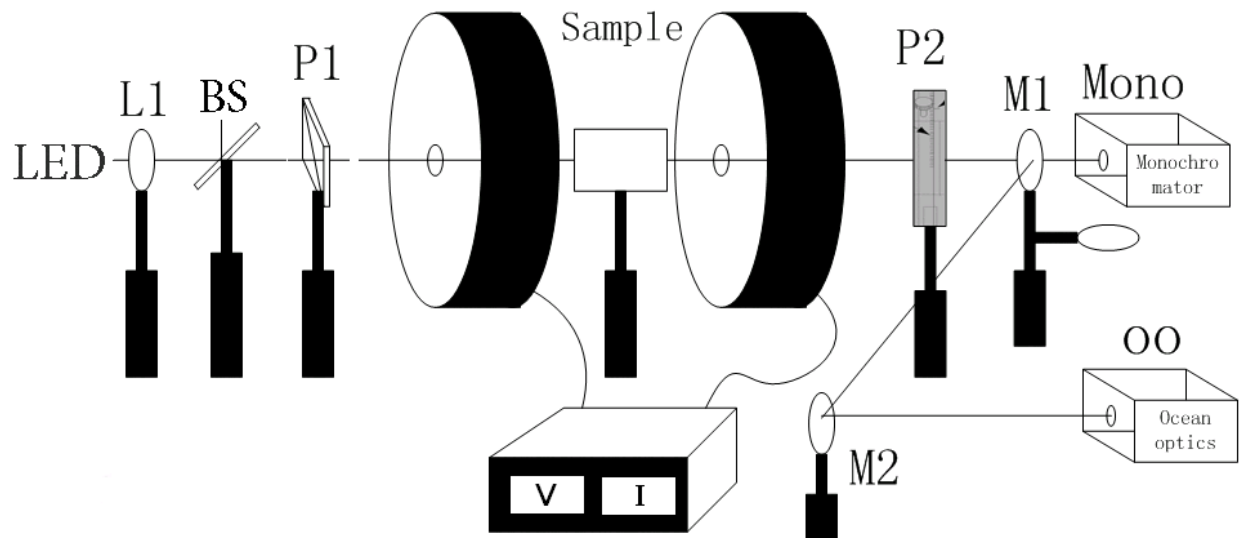


Figure 3.

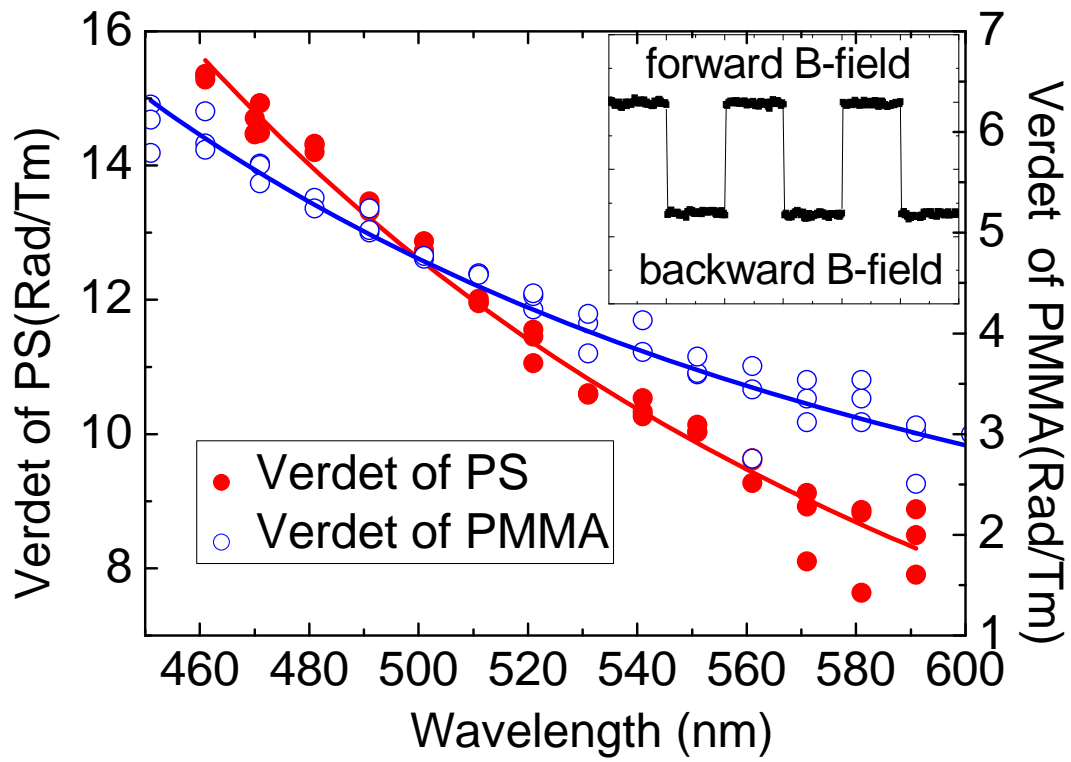


Figure 4.

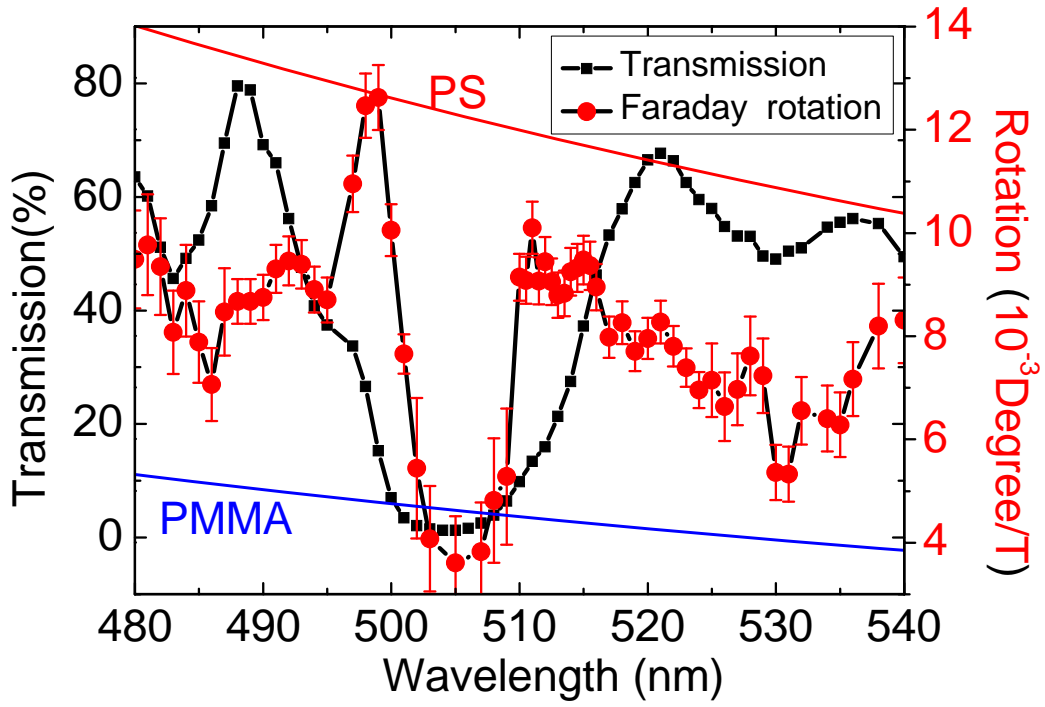


Figure 5.

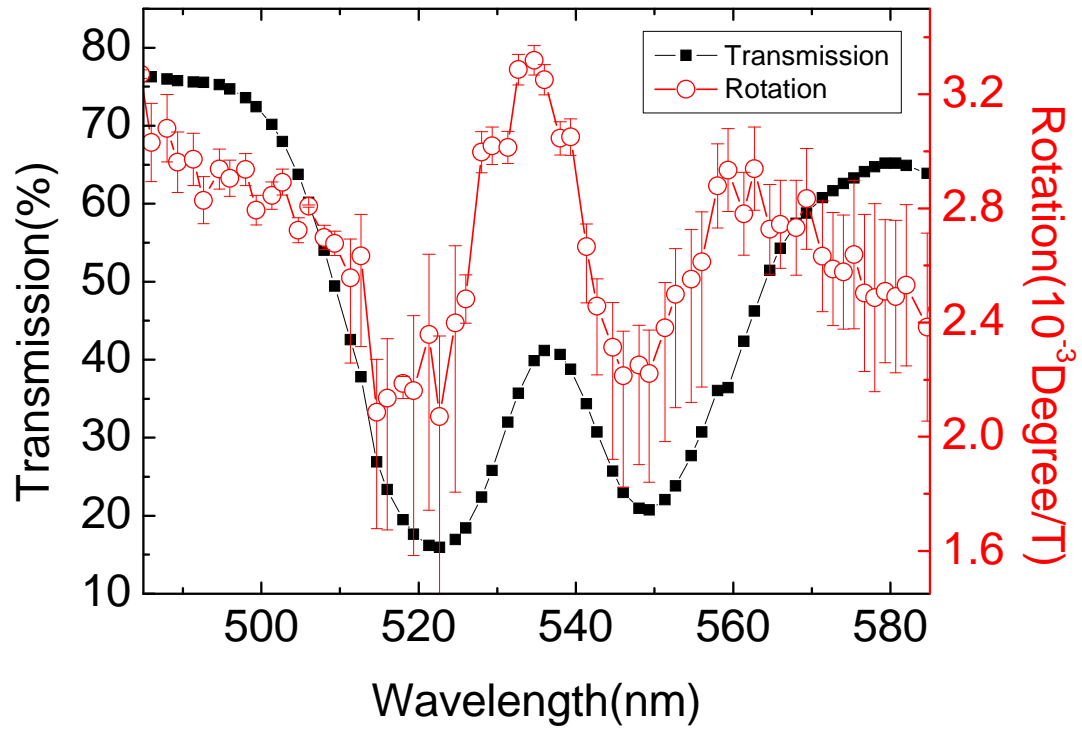


Figure 6.

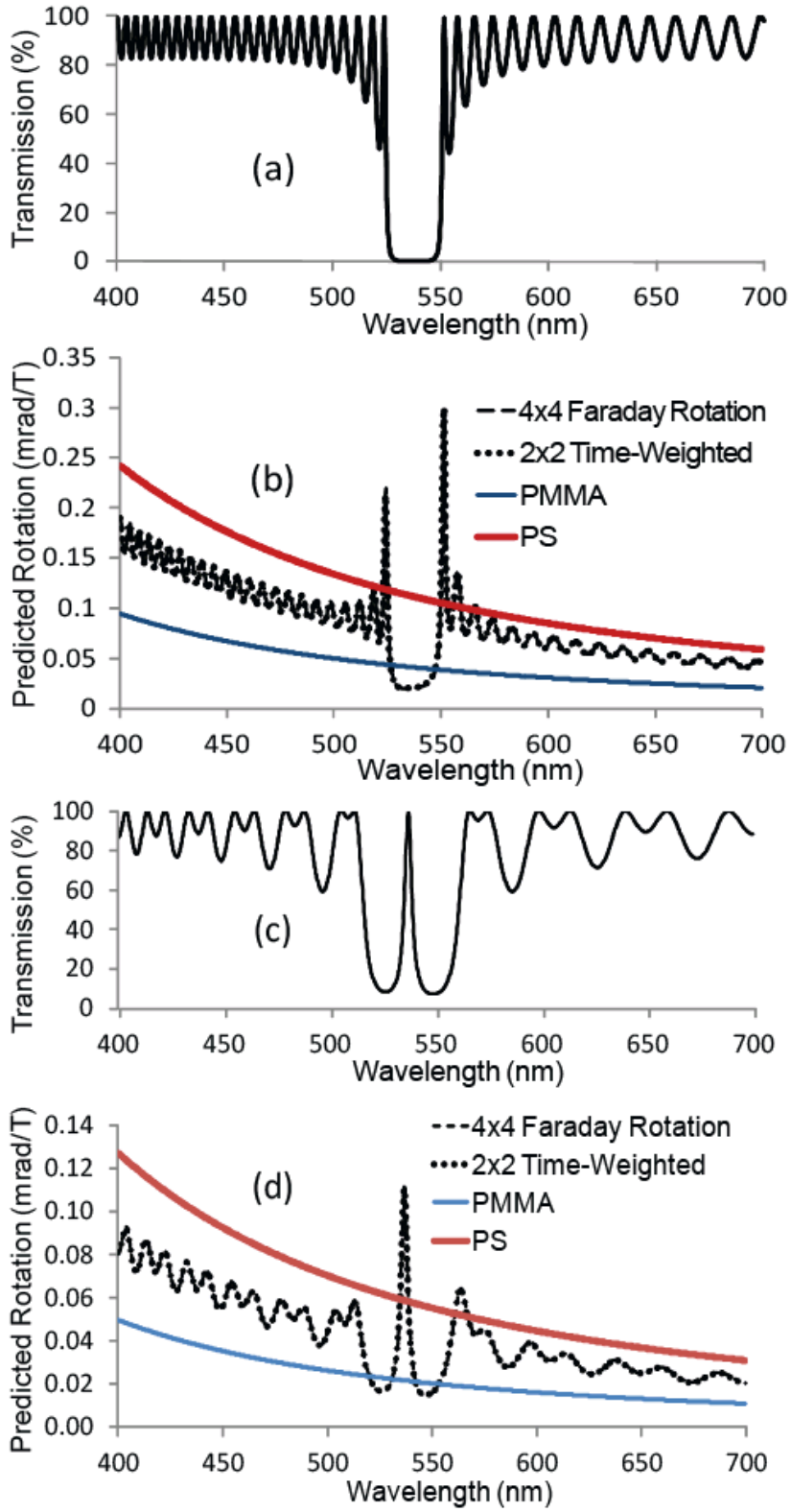


Figure 7.

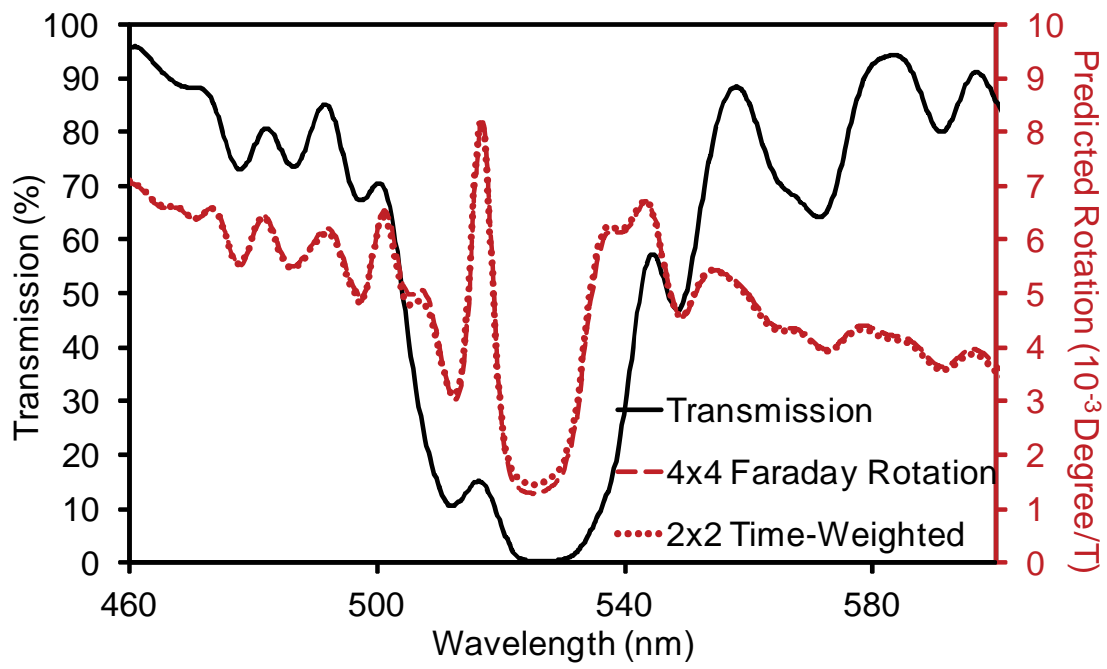


Figure 8.

